NANO LETTERS

pubs.acs.org/NanoLett Letter

Observing Axial Chirality of Chiral Single-Wall Carbon Nanotubes by Helicity-Dependent Raman Spectra

Shiyi Han, Nguyen Tuan Hung, Ying Xie, Riichiro Saito,* Jin Zhang, and Lianming Tong*

Cite This: *Nano Lett.* 2023, 23, 8454−8459 Read Online

ACCESS | Metrics & More | Article Recommendations | Supporting Information

ABSTRACT: Helicity-dependent Raman spectra of an isolated, chiral, single-wall carbon nanotube (SWNT) are reported using circularly polarized light. A polar plot of polarized Raman intensity for the radial breathing mode (RBM), which is excited by left-handed or right-handed circularly polarized light, shows asymmetric angle dependence relative to the nanotube axis direction, which reflects the axial chirality of a SWNT. The asymmetry in the polar plot of the RBM can be analyzed by a complex Raman tensor. The complex phase of each component of the Raman tensor has a maximum at chiral angle $\theta = 15°$ of a SWNT which is between two achiral SWNTs, that is, zigzag ($\theta = 0°$) and armchair ($\theta = 30°$) SWNTs. Considering the interaction between the chiral SWNT and the circularly polarized light, we discuss the origin of the complex phases excited by the opposite helicity of the circularly polarized light.

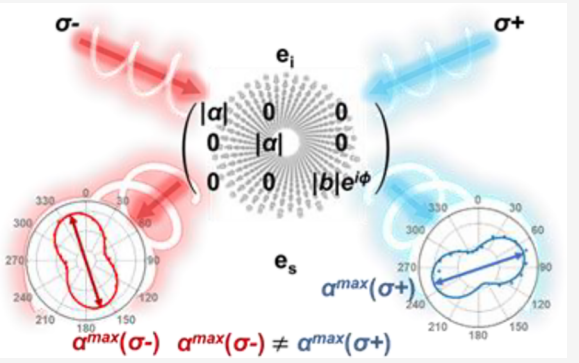

KEYWORDS: *single-wall carbon nanotubes, complex Raman tensor, circularly polarized Raman spectroscopy, handedness*

The structure of a single-wall carbon nanotube (SWNT) is defined by two-integers, namely, the chiral index (n, m). The diameter (d_t) and chiral angle (θ) of a SWNT are given as a function of n and m.[1] If θ is neither 0 nor $\frac{\pi}{6}$ (30°), the nanotube is called a chiral nanotube. In a chiral nanotube, we expect the chiral structure of hexagonal graphene lattice around the nanotube axis whose axial chirality should be maximum at $\theta = \frac{\pi}{12}$ (15°). In this paper, we propose that the helicity-dependent Raman spectra can be used to observe the axial chirality of an isolated chiral SWNT.

The handedness of a chiral SWNT is generally observed by Raman optical activity (ROA) and circular dichroism (CD).[2−4] Margg et al. presented the ROA spectra of enantioenriched SWNTs,[2] Wei et al. measured the CD spectra of the enantiomer-separated SWNTs,[3] and Sato et al. calculated the CD spectra for several values of (n, m) for quantitative comparison of the CD angles.[5] However, it is not easy without theory to discuss the handedness or chiral angle from the ROA and CD in a SWNT dispersion solution. The (n, m) value of SWNTs can be assigned by a Kataura plot using the radial breathing mode (RBM) frequencies obtained by resonant Raman spectroscopy.[1] However, handedness identification and chiral angle determination of an isolated SWNT cannot be achieved by conventional Raman spectroscopy.

In helicity-dependent Raman spectroscopy, left-handed or right-handed circularly polarized light ($\sigma+$ or $\sigma-$) is employed as the incident light, with the scattered light set as helicity-resolved. $\sigma+$ ($\sigma-$) is defined as an integer +1 (−1), which is the spin angular moment of a photon in units of $\hbar$. Since $\sigma+$ and $\sigma-$ are mirror symmetric with each other as well as L-SWNTs and R-SWNTs, we expect to measure the handedness through the chirality by helicity-dependent Raman spectroscopy.

When a material has rotational symmetry around an axis, the Raman-active phonon modes become either helicity-conserved or helicity-changing modes. In the helicity-conserved (helicity-changing) modes, the scattered circularly polarized light has the same (opposite) helicity as the incident circularly polarized light. For example, the A_{1g} mode of MoS_2, which is an out-of-plane mode, is a helicity-conserved mode, while the in-plane E_g mode becomes a helicity-changing mode.[6] Whether the Raman active mode is helicity-conserved or helicity-changing can be understood by Raman intensity calculation using Raman tensors.[7,8] The nature of helicity-dependent Raman scattering is understood by the conservation of pseudoangular momentum of circularly polarized light for the material with n-fold rotational symmetry ($n = 2, 3, 4, 6$).[9]

When a material does not have a mirror symmetry with a mirror that contains the propagation direction of circularly polarized light, the polar plot of Raman intensity after passing the quarter-wave plate becomes asymmetric for $\sigma+$ and $\sigma-$. In

Received: May 15, 2023
Revised: September 3, 2023
Published: September 13, 2023

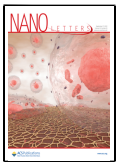

https://doi.org/10.1021/acs.nanolett.3c01791
Nano Lett. 2023, 23, 8454−8459

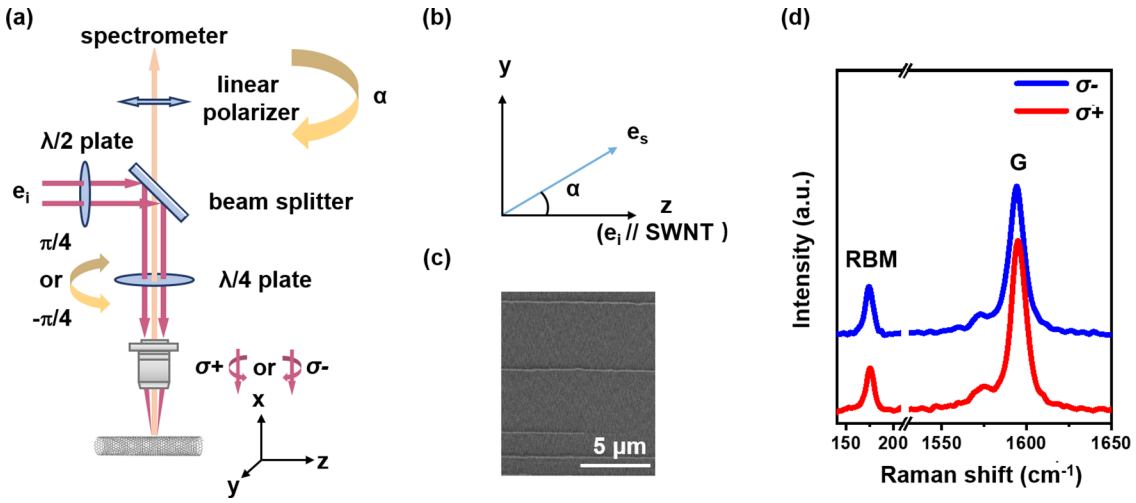

Figure 1. Helicity-dependent Raman spectroscopy of an individual single-walled carbon nanotube (SWNT). (a) Experimental setup for circularly polarized Raman scattering spectroscopy. (b) Coordinate system for the experimental measurements. The SWNTs in a horizontal array are placed parallel to the linear polarization of the incident light before it passes through the quarter-wave plate. An angle α is defined as a variable by the direction of linear polarizer relative to the nanotube axis. (c) Scanning electron microscopy (SEM) image of an SWNT array. (d) Raman spectra of an individual SWNT excited by left- ($\sigma+$) and right-circularly polarized ($\sigma-$) incident light without a linear polarizer for laser excitation energy E_L = 2.33 eV. The peak positions of the radial breathing mode (RBM) are both at 175.7 cm^{-1}, and the chiral index of the SWNT is assigned to (15, 5) according to the Kataura plot.

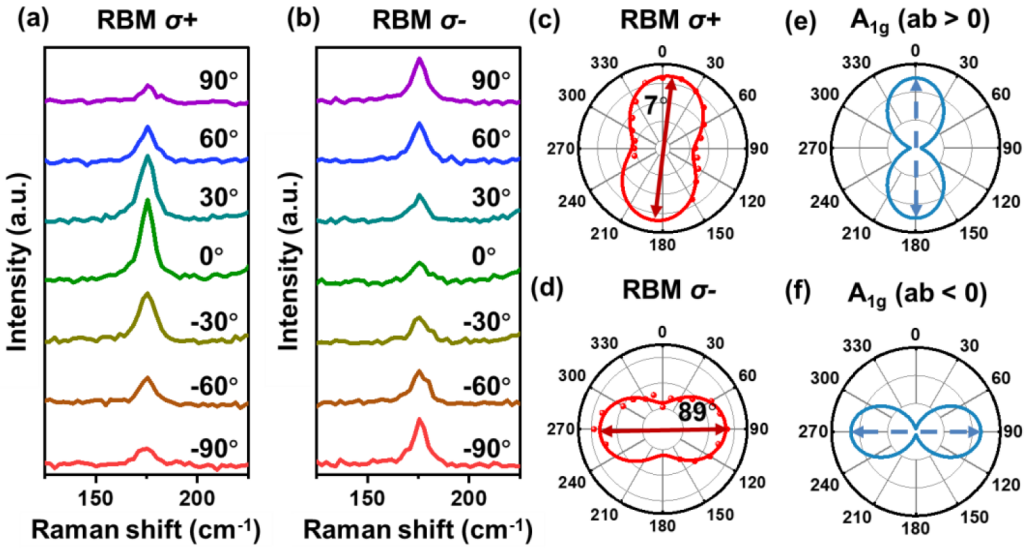

Figure 2. Polarized Raman spectra of the RBM mode of a (15, 5) SWNT as a function of the polarization angle α for incident (a) $\sigma+$ and (b) $\sigma-$ for E_L = 2.33 eV. Polar plots of Raman intensity as a function of α for the RBM mode excited by (c) $\sigma+$ and (d) $\sigma-$. The red dots are the measured Raman intensities to which the red lines are fitted by (c) eq 7 and (d) eq 8, respectively. The red arrow shows the maximum intensity direction of each polar plot. Calculated polar plots of RBM intensities as a function of α for a Raman tensor given in eqs 3 or 4 with (e) $ab > 0$ and (f) $ab < 0$. The dashed arrow shows the long axis of each polar plot.

this case, we need to consider the complex Raman tensor in which each tensor element has its own complex phase. Ribeiro et al. have introduced the complex Raman tensor in linearly polarized Raman spectroscopy of black phosphorus, which illustrates the origin of the complex values by the electron−phonon matrix elements and the energy denominator.[10] In a previous work, we measured helicity-dependent Raman spectra of black phosphorus excited by the circularly polarized light and explained by complex Raman tensor.[11]

In this letter, we adopt the concept of a complex Raman tensor to isolated chiral SWNTs. Similarly to the circularly polarized Raman spectroscopy of black phosphorus, the long axis of the polar plot of the Raman intensity as a function of the polarization for the scattered light deflects from 0/180° or 90/270°. Besides, the polar plot of the RBM of the same SWNT shows a helicity-dependent asymmetric pattern relative to the nanotube-axis direction (the same as the polarization of the incident light), which may reflect the chiral structure and handedness of chiral SWNTs. The observed asymmetry becomes a maximum at $\theta = \frac{\pi}{12}(15°)$, which is consistent with our expectation. We also found that the G band of SWNT shows the nearly symmetric pattern for $\sigma+$ and $\sigma-$ with respect to the nanotube axis. We will discuss the chiral angle dependence of the phenomena by measuring many SWNTs.

https://doi.org/10.1021/acs.nanolett.3c01791
Nano Lett. 2023, 23, 8454−8459

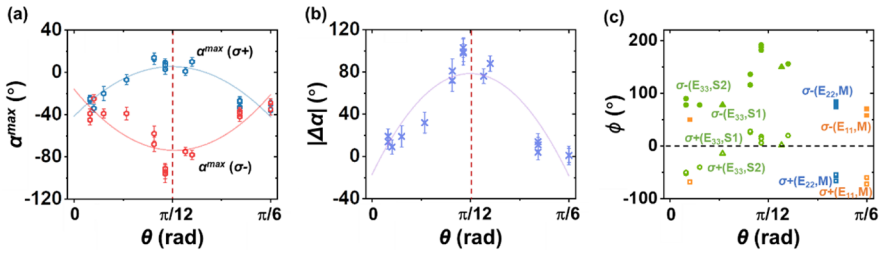

Figure 3. (a) $\alpha^{max}(\sigma+)$ and $\alpha^{max}(\sigma-)$ of the RBM mode as a function of the chiral angle θ of SWNTs. The blue and red lines are the fitting curves for $\alpha^{max}(\sigma+)$ and $\alpha^{max}(\sigma-)$, respectively. (b) Relationship between $|\Delta\alpha| \equiv |\alpha^{max}(\sigma+) - \alpha^{max}(\sigma-)|$ and the chiral angle θ. The red dashed vertical lines in both (a) and (b) refer to $\theta = \frac{\pi}{12}(15°)$. (c) Phase difference ϕ of the complex Raman tensor for RBM as a function of chiral angle θ. Open (solid) symbols, of orange squares, blue squares, green triangles, and green circles denote respectively the value ϕ in degrees for $\sigma+$ ($\sigma-$) at $E_L = E_{11}$ (metal), E_{22} (metal), E_{33} (type I semiconductor, S1), and E_{33} (type II semiconductor, S2) SWNTs. The black horizontal dashed line refers to $\phi = 0°$.

The experimental setup of circularly polarized Raman spectroscopy is shown in Figure 1a. The half-wave plate ($\lambda/2$) is placed in the optical path of the incident light so that the linear polarization of the laser can be rotated to be parallel to the nanotube axis direction. The quarter-wave plate ($\lambda/4$) is placed in the common optical path, and it is rotated until the angle between the optical axis and the z axis is $\pm\frac{\pi}{4}$ to generate either $\sigma+$ or $\sigma-$ as the incident light for excitation. The propagation direction of light is parallel to the x axis, and SWNTs are on the yz plane. See Figure S1 in the Supporting Information for the detailed procedure.

In Figure 1b, we define the angle α as a variable in the yz plane between the direction of the linear polarizer and the z axis. To determine whether the Raman-active mode is helicity-conserved or helicity-changing, the linear polarizer is rotated in the direction perpendicular (parallel) to the z axis to obtain helicity-conserved (helicity-changing) Raman spectra. Thus, $\alpha = \frac{\pi}{2}$ or $-\frac{\pi}{2}$ (α = 0 or π) would correspond to helicity-conserved (helicity-changing) Raman spectra.

Horizontal SWNT arrays were grown by a chemical vapor deposition (CVD) method and were transferred onto a 90 nm SiO_2/Si substrate. Figure 1c shows the scanning electron microscopy (SEM) image of a SWNT array, where the separation between two adjacent SWNTs is larger than the diameter of the laser spot (~1 μm). Without a linear polarizer in the setup, the Raman spectra excited by $\sigma+$ and $\sigma-$ incident lights show identical spectra, as shown in Figure 1d. The peak positions of RBM excited by $\sigma+$ and $\sigma-$ for E_L = 2.33 eV are both 175.7 cm^{-1}. By using the Kataura plot[12] (see details in the Supporting Information), the chiral index and the chiral angle θ of the SWNT are assigned to (15, 5) and 13.9°, respectively.

When we put a linear polarizer for collection in the setup, polar plots of the Raman intensity as a function of α show a distinct angle dependence between $\sigma+$ and $\sigma-$, as shown in Figure 2. In Figure 2a,b, we plot the Raman spectra of the (15, 5) SWNT excited by $\sigma+$ and $\sigma-$, respectively, for several values of α. Here, the laser excitation energy is E_L = 2.33 eV, which is resonant to the E_{33} van Hove singularity energy of joint density of states of the (15, 5) SWNT.[12] In Figure 2c–f, we show polar plots of the Raman intensity as a function of α, excited by $\sigma+$ and $\sigma-$. The red dots in Figure 2c,d are the measured Raman peak intensity by $\sigma+$ and $\sigma-$, respectively. We fit the data with solid red lines to the Raman tensor calculation, as shown in eqs 7 and 8. When the SWNT is excited by $\sigma+$, the maximum intensity appears at α^{max} = 7°, while for $\sigma-$, the maximum intensity appears at α^{max} = 89°, where α^{max} is shown in units of degree (deg) for convenience, and it is sufficient to define $-90° \le \alpha^{max} \le 90°$. Since the SWNT is excited by circular polarization, the polar plots in Figure 2c–f are not related to the antenna effect in SWNTs for explaining the fact that α^{max} values lie in the region from 0 to 90° for 17 observed SWNTs (Figure 3a). In the following, we explain how to fit the observed polar plots by the Raman tensor calculation.

The Raman intensity I is calculated by a given Raman tensor R as follows:

$$I(\sigma_s, \sigma_i) \propto |\sigma_s^{\dagger} \cdot R \cdot \sigma_i|^2 \tag{1}$$

where σ_i ($\sigma_s^{\dagger}$) denotes the Jones vector of the incident (scattered) light (see details in Section 3.1 in the Supporting Information).

Since the RBM is in the A_g mode, according to the group theory, the Raman tensor of the A_g mode (x^2+y^2, or z^2) can be expressed as follows:[13,14]

$$R_{A_g} = \begin{pmatrix} a & 0 & 0 \\ 0 & a & 0 \\ 0 & 0 & b \end{pmatrix} \tag{2}$$

Using eqs 1 and 2 and eqs S16–S23, the Raman intensity of the A_g mode excited by $\sigma+$ and $\sigma-$ can be respectively written as a function of α:

$$I_{A_g}(\sigma+) = a^2 + b^2 + 2ab\cos(2\alpha) \tag{3}$$

$$I_{A_g}(\sigma-) = a^2 + b^2 + 2ab\cos(2\alpha) \tag{4}$$

If we assume that a and b are real numbers, $I_{A_g}(\sigma+)$ and $I_{A_g}(\sigma-)$ would have the same α dependence, which is not consistent with Figure 2c,d. In Figure 2e,f, we show the calculated polar plot of the Raman intensities as a function of α according to eq 3 (eq 4) for $ab > 0$ and $ab < 0$, respectively. It can be seen that α_{max} (blue arrow) becomes either 0/180° ($ab > 0$) or 90/270° ($ab < 0$). In order to explain Figure 2c,d, the sign of ab should be opposite for incident $\sigma+$ and $\sigma-$. It is important to stress that the absolute values of a and b should not depend on $\sigma+$ or $\sigma-$ since a and b are intrinsic values of a SWNT.

To explain the phenomenon, we introduce the complex form of the Raman tensor:

https://doi.org/10.1021/acs.nanolett.3c01791
Nano Lett. 2023, 23, 8454–8459

$$R_{A_g} = \begin{pmatrix} |a|e^{i\phi_a} & 0 & 0 \\ 0 & |a|e^{i\phi_a} & 0 \\ 0 & 0 & |b|e^{i\phi_b} \end{pmatrix} \quad (5)$$

Here we assume that the phases ϕ_a and ϕ_b depend on $\sigma+$ and $\sigma-$. To simplify, we define a phase difference ϕ as

$$\phi(\sigma+) = \phi_b(\sigma+) - \phi_a(\sigma+)$$
$$\phi(\sigma-) = \phi_b(\sigma-) - \phi_a(\sigma-) \quad (6)$$

Thus, the Raman intensities excited by $\sigma+$ and $\sigma-$ can be respectively rewritten as

$$I_{A_g}(\sigma+) \propto |a|^2 + |b|^2 + 2|a||b| \cos(2\alpha(\sigma+) + \phi(\sigma+)) \quad (7)$$

$$I_{A_g}(\sigma-) \propto |a|^2 + |b|^2 + 2|a||b| \cos(2\alpha(\sigma-) - \phi(\sigma-)) \quad (8)$$

It is noted that eq 3 (eq 4) is a special case of eq 7 (eq 8) when $\phi = 0$ (in the case that $ab > 0$).

From eqs 7 and 8, if we define α^{max} as the angle for the maximum intensity, the phase difference ϕ can be calculated by α^{max}:

$$\phi(\sigma+) = -2\alpha^{max}(\sigma+) \quad \phi(\sigma-) = 2\alpha^{max}(\sigma-) \quad (9)$$

From Figure 2c,d, we get $\alpha^{max}(\sigma+) = 7°$ and $\alpha^{max}(\sigma-) = 89°$. It is reasonable that $\phi(\sigma+)$ and $\phi(\sigma-)$ are not the same since the phase factor in the Raman tensor depends on the complex matrix elements of electron−photon and electron−phonon interaction.[11] In the following, we investigate $\alpha^{max}(\sigma+)$ and $\alpha^{max}(\sigma-)$ as a function of chiral angle, θ, by measuring multiple SWNTs. The results for the G band are shown in Figure S3 and discussed in the Supporting Information.

In Figure 3a, we plot $\alpha^{max}(\sigma+)$ and $\alpha^{max}(\sigma-)$ for RBM as a function of the chiral angle θ for 17 individual SWNTs which are resonant to $E_L = 1.96$ or 2.33 eV. The results are fitted by $\alpha^{max} = A(\theta - C)^2 + B$, which are shown as blue and red solid curves for $\alpha^{max}(\sigma+)$ and $\alpha^{max}(\sigma-)$, respectively. It is shown that (1) $\alpha^{max}(\sigma+)$ ($\alpha^{max}(\sigma-)$) has a maximum (minimum) at $\theta = \frac{\pi}{12}$ (15°) and (2) $\alpha^{max}(\sigma+)$ and $\alpha^{max}(\sigma-)$ have almost the same values at $\theta = 0$ and $\frac{\pi}{6}$ (30°). In Figure 3b, we plot $|\Delta\alpha|$ as a function of θ, where $|\Delta\alpha|$ is defined as $|\Delta\alpha| \equiv |\alpha^{max}(\sigma+) - \alpha^{max}(\sigma-)|$. Since $\theta = 0$ and $\frac{\pi}{6}$ (0 and 30°) respectively correspond to zigzag and armchair achiral SWNTs, we expect that the origin of $\alpha^{max}(\sigma+)$ and $\alpha^{max}(\sigma-)$ may come from the chiral structure in the chiral SWNTs whose effect should be the maximum at $\theta = \frac{\pi}{12}$(15°). The results for the G band are shown in Figure S4, where a slight change of α^{max} with θ was observed (see the details in the Supporting Information). Figure 3c shows the phase difference ϕ of the complex Raman tensor for the RBM of 17 SWNTs that we measured as a function of chiral angle θ, which is calculated by eq 9. We can see in Figure 3c that ϕ has a broad maximum for both $\sigma+$ and $\sigma-$. When we consider a mirror symmetry operation with a mirror that contains the nanotube axis, (1) $\sigma+$ and $\sigma-$ and (2) left- and right-enantiomer change simultaneously, the circularly polarized Raman spectroscopy would not change. Specifically, the mirror symmetry operation of the light is equivalent to the mirror symmetry of the SWNT. Thus, we expect that the phase difference between left and right enantiomers is identical to the phase difference between $\sigma+$ and $\sigma-$.

We should mention here that it is beyond the scope of the present paper that we directly calculate ϕ_a and ϕ_b for each SWNT from theoretical calculations of electron−photon and electron−phonon matrix elements for each (n, m). In the resonant Raman spectra, the ij $(i,j = x,y,z)$ component of the Raman tensor is expressed by the products of two electron−photon matrix elements in i and j components and one electron−phonon matrix element for a given phonon mode with two energy denominators.[15] The electron−photon matrix elements are generally complex numbers as a function of the wavevector of a photoexcited electron, and the electron−phonon matrix element can be a complex number. In fact, we theoretically predicted that RBM oscillation starts either shrinking or expanding depending on type I or type II of SWNTs, whose phases of oscillation are different by π, where types I and II are defined by mod$(2n+m, 3) = 1, 2$ for (n, m) SWNT.[16] Further, since the common energy denominator, $(E_f - E_i - \hbar\omega) + i\gamma$, where E_f, E_i, and $\hbar\omega$ denote respectively the energies of the initial and final states and the laser excitation energy, has a complex broadening factor, $i\gamma$; this phase should depend on the relative energy of energy separation $(E_f - E_i)$ to $\hbar\omega$. In the case of a SWNT, a resonant $(E_f - E_i)$ corresponds to van Hove singular energy, E_{ii} $(i = 1, 2, 3, ...)$. Thus, although we do not calculate the complex numbers of the matrix elements, it is interesting to see how ϕ_a and ϕ_b change as a function of E_{ii} relative to the laser excitation energy.

Resende et al. and Pimenta et al. discussed the possible change of the phase of complex Raman tensors, which appears in the broadening factor in the energy denominators.[17,18] However, since this broadening factor is not helicity-dependent, we do not expect that it is the origin of the helicity-dependent phases. We expect that the origin of helicity-dependent phases of the Raman tensor comes from the electron−photon matrix element in which the position-dependent phases of the vector potential on the carbon atoms on a chiral SWNT over the wavelength do not give a one-to-one correspondence for left-handed and right-handed circularly polarized light. It is noted that the position-dependent phases of vector potential on the carbon atoms on a chiral SWNT over the wavelength is essential for explaining the circular dichroism of a chiral nanotube.[5]

In Figure S5, the phase factors are plotted as a function of E_{ii} which is calculated by an exciton Kataura plot[19,20] vs the corresponding energy band gaps that the laser excites. It is seen that for 5 metallic chiral SWNTs, either E_{11} or E_{22} is resonant, and $\phi(\sigma+)$ and $\phi(\sigma-)$ appear in a symmetric position around $\phi = 0$. To specify, the absolute values of $\phi(\sigma+)$ and $\phi(\sigma-)$ are almost the same, which does not depend on E_{ii} below 1.96 eV laser excitation. On the other hand, for 12 semiconducting chiral SWNTs, E_{33} is resonant, and the values of $\phi(\sigma+)$ and $\phi(\sigma-)$ significantly change as a function of E_{ii}, which is consistent with our speculation. It is noted that no specific distinction between type I and II semiconducting SWNTs is found. A possible reason the metallic chiral SWNTs do not show E_{ii} dependence of $\phi(\sigma+)$ and $\phi(\sigma-)$ might be (1) all metallic E_{ii} values are below 1.96 eV or (2) the dependence might be canceled by two contributions from the split E_{11} (or E_{22}) to E_{11}^H and E_{11}^L due to the trigonal warping effect.[21] We cannot explain well the reason types I and II give similar $\phi(\sigma+)$ and $\phi(\sigma-)$. More experiments with many (n, m) SWNTs and theoretical calculations of complex Raman tensors as a

https://doi.org/10.1021/acs.nanolett.3c01791
Nano Lett. 2023, 23, 8454−8459

function of laser energy and (n, m) are needed, which should be conducted in the future.

Let us briefly mention a confusing point on the helicity-dependent Raman spectra of SWNTs. The A_g mode is generally helicity-conserved mode for materials like MoS_2.[8] In Figure 2c, the intensity of the RBM for $\sigma+$ excitation is the highest at $\alpha^{max} = 7°$, which is nearly characteristic of the helicity-changing mode. However, for $\sigma-$ excitation, the maximum intensity appears at $\alpha^{max} = 89°$, which is nearly characteristic of a helicity-conserved mode. This can be explained by the complex Raman tensor. By putting $\alpha = 0$ and $\frac{\pi}{2}$ to eqs 7 and 8, the helicity-conserved and helicity-changing Raman intensities, $I_{\sigma_s\sigma_i}$, are defined for $\sigma_i = \sigma+$:

$$I_{\sigma+\sigma+} = |a|^2 + |b|^2 - 2|a||b| \cos(\phi(\sigma+)) \quad (10)$$

$$I_{\sigma-\sigma+} = |a|^2 + |b|^2 + 2|a||b| \cos(\phi(\sigma+)) \quad (11)$$

Similarly, for $\sigma_i = \sigma-$, we get

$$I_{\sigma-\sigma-} = |a|^2 + |b|^2 - 2|a||b| \cos(\phi(\sigma-)) \quad (12)$$

$$I_{\sigma+\sigma-} = |a|^2 + |b|^2 + 2|a||b| \cos(\phi(\sigma-)) \quad (13)$$

The proportion of helicity-conserved and helicity-changing Raman intensities for $\sigma_i = \sigma+$ and $\sigma-$ is defined in Section 3.2 in the Supporting Information. Using eqs 10−13, the difference between helicity-conserved and helicity-changing Raman intensity $\Delta P(\sigma+)$ and $\Delta P(\sigma-)$ excited by $\sigma+$ and $\sigma-$, respectively, can be expressed by

$$\Delta P(\sigma+) = \frac{I_{\sigma+\sigma+} - I_{\sigma-\sigma+}}{I_{\sigma-\sigma+} + I_{\sigma+\sigma+}} = \frac{-2|a||b|(\cos\phi(\sigma+))}{|a|^2 + |b|^2} \quad (14)$$

$$\Delta P(\sigma-) = \frac{I_{\sigma-\sigma-} - I_{\sigma+\sigma-}}{I_{\sigma+\sigma-} + I_{\sigma-\sigma-}} = \frac{-2|a||b|(\cos\phi(\sigma-))}{|a|^2 + |b|^2} \quad (15)$$

It is clear from eqs 14 and 15 that $\Delta P(\sigma+)$ and$\Delta P(\sigma-)$ depend on ϕ. In Figure 4a, we plot $\Delta P(\sigma+)$ and $\Delta P(\sigma-)$ as a function of chiral angle θ, which shows that the helicity-selection rule of the RBM mode is affected by the helicity of the incident light and the chiral angle of a SWNT. In Figure 4b, we plot ΔP as a function of chiral angles, where we define ΔP by $\Delta P \equiv \Delta P(\sigma+) - \Delta P(\sigma-)$. The minimum of ΔP appears at chiral angle $\theta = \frac{\pi}{12}$.

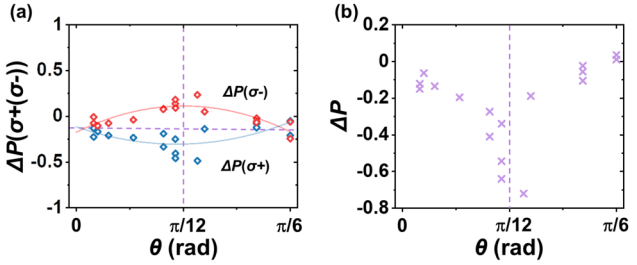

Figure 4. (a) $\Delta P(\sigma+)$ and $\Delta P(\sigma-)$ as functions of chiral angle θ. The red (blue) button represents the SWNT excited by $\sigma+$ and $\sigma-$, respectively. (b) ΔP as a function of chiral angle θ for RBM. The vertical dashed line corresponds to $\theta = \frac{\pi}{12}$, and the horizontal dashed line in (a) refers to the mean values of ΔP.

Finally, let us mention the handedness of SWNTs. When we imagine the mirror operation to the experiment with the mirror in the xz plane, the incident helicity of circularly polarized light and handedness of a SWNT change at the same time, and the phenomena give the same absolute values of $\phi(\sigma+)$ and $\phi(\sigma-)$ with the opposite signs. Thus, it would be very interesting to measure $\phi(\sigma+)$ and $\phi(\sigma-)$ for an enantiomer pair (n, m) and $(n + m, -m)$ to confirm the present measurement. Although we have measured 17 SWNTs, we could not find any evidence that we have measured both enantiomers of (n, m) and $(n + m, -m)$ for a given (n, m). We do not know if the original SWNT sample has only one enantiomer type or not. It is highly desirable to measure the well-defined enantiomer pair of SWNTs to verify the present phenomena.

In this work, we report the circularly polarized Raman spectra of isolated SWNTs. The polarized Raman intensity of the RBM as a function of the linear-polarizer angle for scattered light gives asymmetric angles of the maximum Raman intensity $\alpha^{max}(\sigma+)$ and $\alpha^{max}(\sigma-)$ which depend on the helicity of incident circularly polarized light ($\sigma+$ or $\sigma-$). The absolute values of the difference $|\Delta\alpha| \equiv |\alpha^{max}(\sigma+) - \alpha^{max}(\sigma-)|$ for 17 SWNTs have a maximum at the chiral angle of a SWNT, $\theta = \frac{\pi}{12}$, which suggests the effect of chiral structure of each SWNT. The phenomena can be explained by a complex Raman tensor in which the difference of phase factors between two complex elements of the Raman tensor depends on the chiral angle and helicity of the incident light. Although the present measurement is not directly calculated by theoretical calculations, we have proposed a new method to measure the chiral angle and handedness of a SWNT, which can be applied to any chiral material.

■ ASSOCIATED CONTENT

Supporting Information

The Supporting Information is available free of charge at https://pubs.acs.org/doi/10.1021/acs.nanolett.3c01791.

Experimental methods, including sample preparation, Raman scattering measurements, SEM measurements, and experimental procedure, experimental setup to determine the nanotube axis, line shapes of the G band, polarized Raman spectra of the G band of (15, 5) SWNT at different α angles and the polar plots of G band intensities as a function of α, $\alpha^{max}(\sigma+)$, $\alpha^{max}(\sigma-)$, and $|\Delta\alpha|$ of the G band as a function of chiral angle θ of SWNTs, phase difference ϕ for the RBM as a function of electronic transition energies (E_{ii}), Raman tensor calculation, and the Jones vector of the quarter-wave plate and the proportion of helicity-conserved and helicity-changing Raman intensities for $\sigma_i = \sigma+$ and $\sigma-$ (PDF)

■ AUTHOR INFORMATION

Corresponding Authors

Riichiro Saito − *Department of Physics, Tohoku University, Sendai 980-8578, Japan*; Email: r.saito.sendai@gmail.com

Lianming Tong − *College of Chemistry and Molecular Engineering, Beijing Science and Engineering Center for Nanocarbons, Beijing National Laboratory for Molecular Sciences, Peking University, Beijing 100871, People's Republic of China*; orcid.org/0000-0001-7771-4077; Email: tonglm@pku.edu.cn

https://doi.org/10.1021/acs.nanolett.3c01791
Nano Lett. 2023, 23, 8454−8459

Authors

Shiyi Han − *College of Chemistry and Molecular Engineering, Beijing Science and Engineering Center for Nanocarbons, Beijing National Laboratory for Molecular Sciences, Peking University, Beijing 100871, People's Republic of China*

Nguyen Tuan Hung − *Frontier Research Institute for Interdisciplinary Science, Tohoku University, Sendai 980-8578, Japan;* orcid.org/0000-0003-4156-6230

Ying Xie − *College of Chemistry and Molecular Engineering, Beijing Science and Engineering Center for Nanocarbons, Beijing National Laboratory for Molecular Sciences, Peking University, Beijing 100871, People's Republic of China*

Jin Zhang − *College of Chemistry and Molecular Engineering, Beijing Science and Engineering Center for Nanocarbons, Beijing National Laboratory for Molecular Sciences, Peking University, Beijing 100871, People's Republic of China;* orcid.org/0000-0003-3731-8859

Complete contact information is available at: https://pubs.acs.org/10.1021/acs.nanolett.3c01791

Author Contributions

S.H. conceived the idea and designed the experiments. S.H., N.T.H., R.S., and L.T. took part in the experimental data analysis and wrote the manuscript. Y.X. prepared the sample. The work was supervised by R.S., J.Z., and L.T. All the authors discussed the results and commented on the manuscript.

Notes

The authors declare no competing financial interest.

■ ACKNOWLEDGMENTS

The authors thank HORIBA Scientific and Dr. Chunyang Wang for assistance in Raman spectra measurements and thank Dr. Liu Qian and Dr. Tianze Tong for assistance in SWNT array transfer. This work was financially supported by the Ministry of Science and Technology of China (2018YFA0703502 and 2016YFA0200104), the National Natural Science Foundation of China (Grant Nos. 52021006, 51720105003, 21790052, and 21974004), the Strategic Priority Research Program of CAS (XDB36030100), and the Beijing National Laboratory for Molecular Sciences (BNLMS-CXTD-202001). N.T.H. acknowledges a JSPS KAKENHI Grant (No. JP20K15178). R.S. acknowledges a JSPS KAKENHI Grant (No. JP22H00283).

■ REFERENCES

(1) Jorio, A.; Saito, R.; Hafner, J. H.; Lieber, C. M.; Hunter, M.; McClure, T.; Dresselhaus, G.; Dresselhaus, M. S. Structural (*n,m*) Determination of Isolated Single-Wall Carbon Nanotubes by Resonant Raman Scattering. *Phys. Rev. Lett.* **2001**, *86* (6), 1118−1121.

(2) Magg, M.; Kadria-Vili, Y.; Oulevey, P.; Weisman, R. B.; Buergi, T. Resonance Raman Optical Activity Spectra of Single-Walled Carbon Nanotube Enantiomers. *J. Phys. Chem. Lett.* **2016**, *7* (2), 221−225.

(3) Wei, X.; Tanaka, T.; Yomogida, Y.; Sato, N.; Saito, R.; Kataura, H. Experimental determination of excitonic band structures of single-walled carbon nanotubes using circular dichroism spectra. *Nat. Commun.* **2016**, *7* (1), 12899.

(4) Yao, F.; Yu, W.; Liu, C.; Su, Y.; You, Y.; Ma, H.; Qiao, R.; Wu, C.; Ma, C.; Gao, P.; et al. Complete structural characterization of single carbon nanotubes by Rayleigh scattering circular dichroism. *Nat. Nanotechnol.* **2021**, *16* (10), 1073−1078.

(5) Sato, N.; Tatsumi, Y.; Saito, R. Circular dichroism of single-wall carbon nanotubes. *Phys. Rev. B* **2017**, *95* (15), 155436.

(6) Tatsumi, Y.; Kaneko, T.; Saito, R. Conservation law of angular momentum in helicity-dependent Raman and Rayleigh scattering. *Phys. Rev. B* **2018**, *97* (19), 195444.

(7) Chen, S.-Y.; Zheng, C.; Fuhrer, M. S.; Yan, J. Helicity-Resolved Raman Scattering of MoS_2, $MoSe_2$, WS_2, and WSe_2 Atomic Layers. *Nano Lett.* **2015**, *15* (4), 2526−2532.

(8) Drapcho, S. G.; Kim, J.; Hong, X.; Jin, C.; Shi, S.; Tongay, S.; Wu, J.; Wang, F. Apparent breakdown of Raman selection rule at valley exciton resonances in monolayer MoS_2. *Phys. Rev. B* **2017**, *95* (16), 165417.

(9) Tatsumi, Y.; Saito, R. Interplay of valley selection and helicity exchange of light in Raman scattering for graphene and MoS_2. *Phys. Rev. B* **2018**, *97* (11), 115407.

(10) Ribeiro, H. B.; Pimenta, M. A.; de Matos, C. J. S.; Moreira, R. L.; Rodin, A. S.; Zapata, J. D.; de Souza, E. A. T.; Castro Neto, A. H. Unusual Angular Dependence of the Raman Response in Black Phosphorus. *ACS Nano* **2015**, *9* (4), 4270−4276.

(11) Han, S.; Zhao, Y.; Tuan Hung, N.; Xu, B.; Saito, R.; Zhang, J.; Tong, L. Complex Raman Tensor in Helicity-Changing Raman Spectra of Black Phosphorus under Circularly Polarized Light. *J. Phys. Chem. Lett.* **2022**, *13* (5), 1241−1248.

(12) Sato, K.; Saito, R.; Nugraha, A. R. T.; Maruyama, S. Excitonic effects on radial breathing mode intensity of single wall carbon nanotubes. *Chem. Phys. Lett.* **2010**, *497* (1), 94−98.

(13) Saito, R.; Takeya, T.; Kimura, T.; Dresselhaus, G.; Dresselhaus, M. S. Raman intensity of single-wall carbon nanotubes. *Phys. Rev. B* **1998**, *57* (7), 4145−4153.

(14) Dresselhaus, M. S.; Dresselhaus, G.; Eklund, P. C. Chapter 1 - Historical Introduction. In *Science of Fullerenes and Carbon Nanotubes*; Dresselhaus, M. S., Dresselhaus, G., Eklund, P. C., Eds.; Academic Press: 1996; pp 1−14.

(15) Loudon, R. The Raman effect in crystals. *Adv. Phys.* **1964**, *13* (52), 423−482.

(16) Nugraha, A. R. T.; Sanders, G. D.; Sato, K.; Stanton, C. J.; Dresselhaus, M. S.; Saito, R. Chirality dependence of coherent phonon amplitudes in single-wall carbon nanotubes. *Phys. Rev. B* **2011**, *84* (17), 174302.

(17) Resende, G. C.; Ribeiro, G. A. S.; Silveira, O. J.; Lemos, J. S.; Brant, J. C.; Rhodes, D.; Balicas, L.; Terrones, M.; Mazzoni, M. S. C.; Fantini, C.; et al. Origin of the complex Raman tensor elements in single-layer triclinic $ReSe_2$. *2D Mater.* **2021**, *8* (2), 025002.

(18) Pimenta, M. A.; Resende, G. C.; Ribeiro, H. B.; Carvalho, B. R. Polarized Raman spectroscopy in low-symmetry 2D materials: angle-resolved experiments and complex number tensor elements. *Phys. Chem. Chem. Phys.* **2021**, *23* (48), 27103−27123.

(19) Nugraha, A. R. T.; Saito, R.; Sato, K.; Araujo, P. T.; Jorio, A.; Dresselhaus, M. S. Dielectric constant model for environmental effects on the exciton energies of single wall carbon nanotubes. *Appl. Phys. Lett.* **2010**, *97* (9), 091905.

(20) Sato, K.; Saito, R.; Jiang, J.; Dresselhaus, G.; Dresselhaus, M. S. Discontinuity in the family pattern of single-wall carbon nanotubes. *Phys. Rev. B* **2007**, *76* (19), 195446.

(21) Saito, R.; Dresselhaus, G.; Dresselhaus, M. S. Trigonal warping effect of carbon nanotubes. *Phys. Rev. B* **2000**, *61* (4), 2981−2990.